Proceedings of the Canadian Society for Mechanical Engineering International Congress
32nd Annual Conference of the Computational Fluid Dynamics Society of Canada
Canadian Society of Rheology Symposium
CSME/CFDSC/CSR 2025
May 25–28, 2025, Montréal, Québec, Canada

OpenFOAM Simulation of the Gravity Current Front in Submergence on an Incline

Sana Ramezani[1*], Vincent H. Chu[2]

[1,2]Department of Civil Engineering and Applied Mechanics, McGill University, Montreal, Canada
[*] sana.ramezani@mail.mcgill.ca

***Abstract*—**Using a well-calibrated OpenFOAM source code, we conducted a large-eddy simulation (LES) to study the gravity current front produced by a continuous buoyancy source in submergence on an inclined. The LES provides the turbulent velocity and vorticity structures of the current. At the leading edge of the current is a gravity current head developing from the Kelvin-Helmholtz instability. The most significant current occurs at the back of the current head through the neck – which connects the head to the body of the trailing current. We relate the flow through the neck and the turbulent structure of the current head to the buoyancy flux and the slope of the incline. The front velocity obtained from the simulations agrees with the laboratory observation. The current velocity through the neck, not ever measured in the laboratory, is determined from the LES to be 1.94 and 2.22 times greater than the frontal speed for the inline slope angle of 5° and 10°, respectively.

***Keywords-component*—OpenFOAM simulation; gravity current on an incline; coherent turbulence front; turbulent mixing and entrainment**

I. Introduction

Gravity currents occur when dense fluid is released suddenly or continuously into an ambient environment. The buoyancy-driven flows are widely observed in various geophysical scenarios. In coastal and riverine contexts, they are critical in transporting sediment and pollutants and pose significant risks to offshore coastal structures. For instance, turbidity currents can reach velocities of up to 20 m/s, breaking communication cables in the Strait of Luzon off southern Taiwan, associated with the 2006 Pingtung earthquakes as reported by Hsu et al. [1] Heezen and Ewing [2] attributed the earthquake-triggered turbidity currents to successive telegraph cable breaks during the 1929 Grand Banks earthquake. Such events heighten the risks to offshore infrastructure and necessitate stringent safety measures in deep-water construction.

Xie and Chu in 2022 [3], and Ramezani, Xie, and Chu in 2024 [4] studied the impact of Boussinesq and non-Boussinesq gravity current impact on a circular cylinder above the seabed, due a sudden release of dense fluid in a reservoir behind a dam and relate the peak impact force with the arrival of the gravity current head (GCH) – a coherent turbulence structure characterized by a raised head leading a shallower flow behind it. Many studies of the GCH have been on the current on a horizontal bed. However, Britter & Linden in 1980 [6] have examined the gravity currents due to a continuous source on an incline and, with considerable insight, correlated their laboratory-measured speed with the source buoyancy and channel slope.

In this paper, the structural details of the gravity current produced by a continuous source on an incline are determined by a well-calibrated *OpenFOAM*-based LES model previously employed by Xie and Chu [3], and Ramezani, Xie, and Chu [4]. This LES framework has been thoroughly validated in earlier studies. In particular, Xie and Chu [3] applied the model to simulate impact forces from a Boussinesq gravity current—characterized by a small density difference $(\rho_s - \rho_a)/\rho_a = 0.02$— on a circular cylinder above the seabed. That study was based on the Boussinesq approximation, which assumes a constant density but variable specific weight. In a more recent study by Ramezani, Xie, and Chu [4], the model was validated for non-Boussinesq conditions by comparing simulations with the laboratory experiments of Lowe, Rottman, and Linden [5], which involved lock-exchange gravity currents with larger density differences ranging from $(\rho_s - \rho_a)/\rho_a = 0.0526$ to 0.648. The validated LES model is now applied to simulate gravity currents continuously supplied by a source, with a focus on the feeding flow through the

This research is supported by the Natural Sciences and Engineering Research Council of Canada under Grant RGPIN-2019-05776 and a MEDA Scholarship and a FRQNT Scholarship to Sana Ramezani.

neck region that connects the gravity current head (GCH) to the trailing body of the current. We further verify the LES model against existing continuous current experimental data but concentrate our investigation on the neck region, where the feeding velocity sustains the GCH and controls the development of coherent turbulence structures. Notably, this dominant velocity—crucial to the persistence and structure of the GCH—has not been clearly defined in previous laboratory or numerical studies. In this work, no further parameter tuning was performed; the term "well-calibrated" refers to the LES model's prior validation across a wide range of flow conditions, which supports its applicability to the current study.

Therefore, the LES of the continuous source on an incline is to quantify the role of the feeding flow through the neck on the coherent turbulence and the entrainment of ambient fluid into the GCH. By bridging the knowledge gap between laboratory observations and the coherent turbulence dynamics of the GCH under a range of release conditions, we lay the groundwork for future study of impact forces on offshore structures by the continuous current.

II. Numerical Modeling

The schematic in Fig. 1(a) shows the simulation setup. A continuous source of buoyancy flux produces the gravity current, $g'_\circ q_\circ$ across the width of the chamber with a height of $H_\circ$. The inflow has a sludge density ρ_s entering a chamber of height H_T and length L_T filled with ambient fluid of density ρ_a. The reduced gravity is $g'_\circ = g(\rho_s - \rho_a)/\rho_a$. The gravity current propagates down the slope at an angle θ. At the front of the density current is a coherent turbulent front of elevated height known as the gravity current head (GCH), advancing with a frontal velocity u_f. The entrainment of ambient fluid into the GCH is associated with Kelvin–Helmholtz (K-H) vortices, which develop from instabilities originating at the leading edge. The most significant velocity u_m in the back of the GCH through the neck connecting the body of the current exceeds its frontal velocity u_f. The height of the GCH, h_m, is defined as the elevation of the K-H vortex center where vorticity reaches its peak.

A. *twoLiquidMixingFoam Solver*

The numerical simulations relied on an open-source computational fluid dynamic solver known as twoLiquidMixingFoam. The solver and several pre-/post- processing utilities are part of a C++ toolbox maintained in a library that is customized and distributed by the OpenFOAM Foundation ([7], [8]). The solver and several pre-/post-processing utilities are part of a C++ toolbox maintained in a library that is customized and distributed by the OpenFOAM Foundation [7], [8]. Successful implementations of the OpenFOAM solvers for studying coastal and river engineering processes include the works of Higuera, Lara, and Losada [9]–[11] and Nguyen [12]. More recent work used OpenFOAM to study gravity currents, as conducted by Ramezani, Xie, and Chu in 2024 [4], and Xie and Chu in 2022 [3]. The twoLiquidMixingFoam solver, in particular, has been used by Gruber et al. [16] and Krpan and Končar [17] for related fluid dynamic simulations.

The twoLiquidMixingFoam solver models the mixing between the gravity current and its surroundings by determining the volume fraction of one fluid, α, and the fraction of the other fluid, $(1-\alpha)$, by solving the advection-diffusion equation, as described by Krpan and Končar [17].

$$\frac{\partial \alpha}{\partial t} + \frac{\partial u_j \alpha}{\partial x_j} = \frac{\partial}{\partial x_j}[(D_m + \frac{\nu_t}{Sc})\frac{\partial}{\partial x_j}\alpha] \tag{1}$$

where D_m, ν_t and Sc are molecular diffusion coefficient, sub-grid scale eddy viscosity and the sub-grid scale eddy Schmidt number, respectively. The density of the mixed fluid is $\rho = \alpha\rho_s + (1-\alpha)\rho_a$. The velocity vector u_i is determined by the continuity equation and the momentum equation (Gruber et al., 2011 [16]):

$$\frac{\partial \rho}{\partial t} + \frac{\partial}{\partial x_j}(\rho u_j) = 0 \tag{2}$$

$$\frac{\partial \rho u_i}{\partial t} + \frac{\partial}{\partial x_j}(\rho u_i u_j) = -\frac{\partial p}{\partial x_i} + \frac{\partial \tau_{ij}}{\partial x_j} + \rho g \tag{3}$$

The stress τ_{ij} is related to the strain-rate S_{ij} as follows:

$$\tau_{ij} = 2(\nu + \nu_t)S_{ij}, \qquad S_{ij} = \frac{1}{2}\left(\frac{\partial u_i}{\partial x_j} + \frac{\partial u_j}{\partial x_i}\right) \tag{4}$$

where ν and ν_t are the molecular viscosity and the sub-grid scale eddy viscosity, respectively. The spatial discretization of the equations is the linear upwind scheme, except for the volume-fraction equation, which was solved using the VanLeer scheme. We use the PIMPLE iterative algorithm for coupling momentum and mass conservation equations. The number of the corrector was two, as OpenFOAM (2017) [7] recommended. The time integration is by the implicit Euler method. The dynamic time-stepping ensures the local Courant number is less than 0.8.

B. *Subgrid Scale Modelling*

The twoLiquidMixingFoam solver offers many options for the Large-eddy simulation (LES) to determine the sub-grid-scale viscosity. We conducted LES for the impact forces in a previous paper by Xie and Chu [3] and found the dynamicKEquation model ([18], [19]) to produce the best simulation results when compared with the laboratory measurement of the forces by Ermanyuk and Gavrilov [20]. Additionally, we reproduced the front position and velocity of the experimental simulations conducted by Shin, Dalziel, and Linden [21] for Boussinesq currents in our previous simulations ([4]). In the dynamicKEquation model, the sub-grid scale eddy viscosity.

$$\nu_t = C_\nu \Delta k^{0.5} \tag{5}$$

is determined by the numerical solution of dynamicKEquation

$$\begin{aligned}\frac{\partial \rho k}{\partial t} + \frac{\partial \rho u_j k}{\partial x_j} = \frac{\partial}{\partial x_j}\left[\rho\left(\nu + C_\nu \Delta k^{\frac{1}{2}}\right)\frac{\partial k}{\partial x_j}\right] \\ + 2C_\nu \Delta \rho k^{\frac{1}{2}} S_{ij} S_{ij} - \frac{C_\epsilon \rho k^{\frac{3}{2}}}{\Delta}\end{aligned} \tag{6}$$

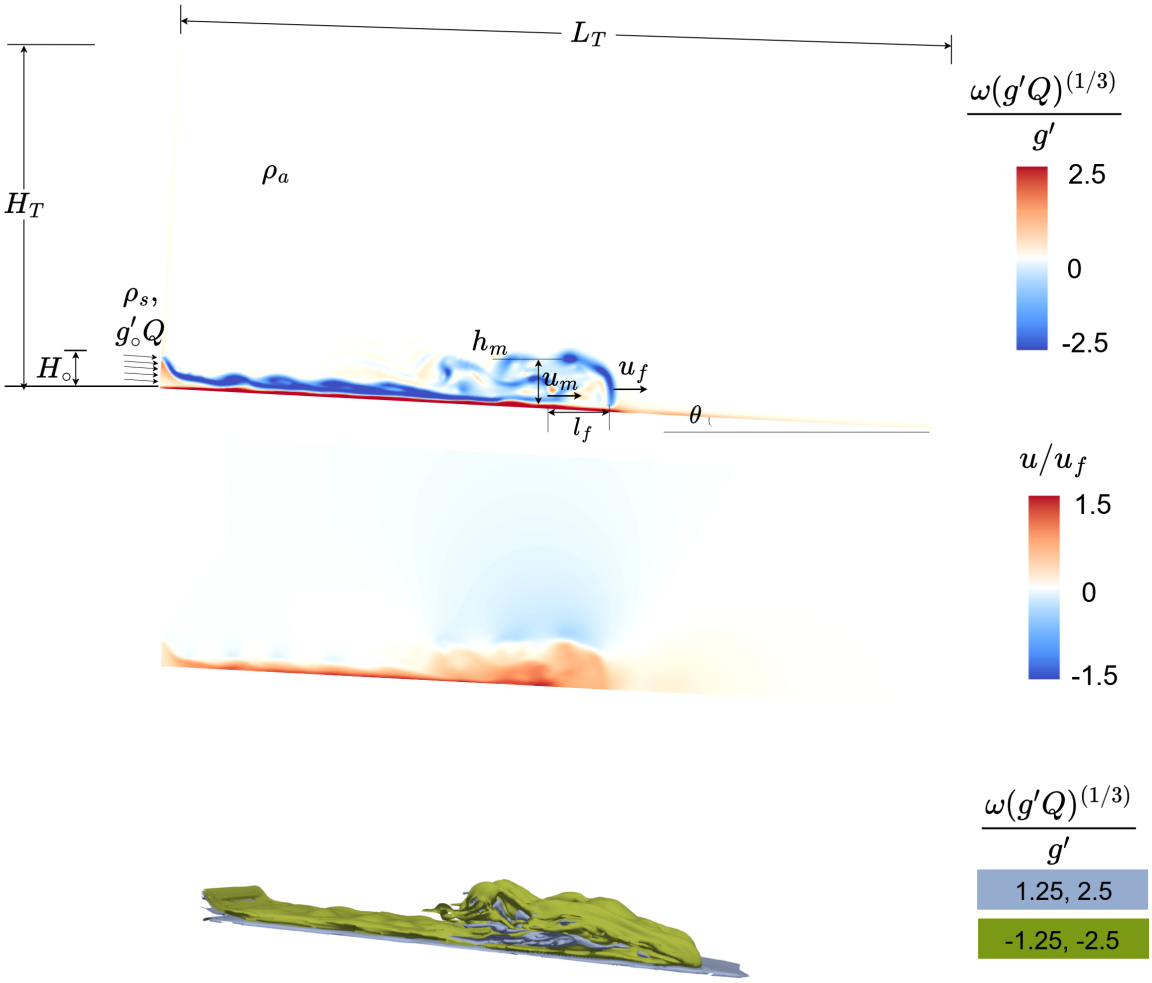

Figure. 1. Gravity current produced by continuous buoyancy flux $g'_\circ q_\circ$ ($\mathrm{cm^3 s^{-3}}$) with density ρ_s induced into an ambient density ρ_a over a slope $\theta = 10°$c. (a) A 2-D iso-vorticity map on the center plan identifies the gravity current head (GCH) connecting to the body of the current through a "neck" where velocity is the maximum u_m greater than the frontal velocity u_f. (b) A u-velocity map showing the occurrence of its maximum at the neck. (c) A 3D- iso-vorticity map identifies the dominant vortices in the GCH. (d) The flow profile $q/q_\circ$. The panels are plotted at $t/t* = 8$ where the frontal position reaches $x_f/l_b = 38.2$. The time scale is $t* = g'/(g'_\circ q_\circ)^{(1/3)}$. The length scale is $l_b = [q_o^2/g']^{\frac{1}{3}}$.

wherein Δ is the mesh size, k is turbulent kinetic energy in the sub-grid scale, and S_{ij} is the resolved strain-rate tensor. C_ν and C_ϵ are dynamically determined during the numerical simulation.The book *Large-Eddy Simulation in Hydraulics* by Rodi, Constantinescu, and Stoesser [22] recommends the use of the dynamicKEquation model for sub-grid-scale modeling of turbulence motion.

C. Computation Mesh

We conducted Large Eddy Simulations (LES) of continuous gravity currents using the same tank dimensions as the laboratory experiments by Britter and Linden [6]. The computational domain has dimensions of height $H_T = 0.6\,\mathrm{m}$, length $L_T = 2.4\,\mathrm{m}$, and width $W_T = 0.15\,\mathrm{m}$. The initial density difference between the brine and ambient fluid in the laboratory experiments by Britter and Linden [6] corresponds

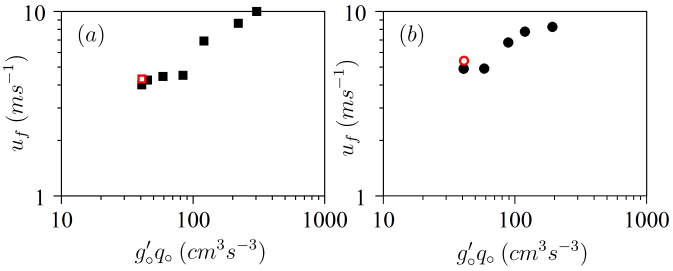

Figure. 2. The frontal velocity u_f (m/s) as a function of buoyancy flux $g'_\circ q_\circ\,(\mathrm{cm^3 s^{-3}})$ in the gravity currents over the inclined slope with (a) $\theta = 5°$, and (b) $\theta = 10°$. The red open denote the LES results, while the black solid symbols denote the laboratory measurements by Britter and Linden [6].

to Boussinesq currents (BC). In our LES, the density difference is set to $(\rho_s - \rho_a)/\rho_a = 0.007$ and imposed buoyancy flux up the slope is $g'_\circ q_\circ = 0.000041\,\mathrm{m}^3/\mathrm{s}^3$. The inlet flow height is $H_\circ = 0.04\,\mathrm{m}$, with an inlet width $W_\circ = W_T = 0.15\,\mathrm{m}$. Simulations were conducted for slopes of $\theta = 5^\circ$ and $\theta = 10^\circ$. The polyMesh utility in the OpenFOAM library is used to generate a hexahedral mesh for the computational domain. The number of cells in the longitudinal, vertical, and transverse directions are $(Nx, Ny, Nz) = (670, 95, 42)$ with $N_{y,\text{inflow}} = 18$. These mesh resolutions were determined following a grid independence study. The dimensionless wall distance y^+ adjacent to all walls is maintained below 1, as recommended in [23]. We apply a no-slip boundary condition on the bottom, sidewalls, and upstream-end wall, while a free-slip boundary condition is imposed on the top wall. The downstream boundary is treated as an outflow boundary condition.

D. Validation of LES for Continuous Gravity Current

We validate our LES results by comparing the simulated frontal velocities with the laboratory experiments conducted by Britter and Linden [6] for continuous gravity currents on varying slopes. Figure 2 presents this comparison for a buoyancy flux of $g'_\circ q_\circ = 0.000041\,(\mathrm{cm}^3\mathrm{s}^{-3})$. The results for $\theta = 5^\circ$ are shown in Fig. 2(a), while Fig. 2(b) corresponds to $\theta = 10^\circ$. Britter and Linden [6] reported frontal velocities of $u_f = 4.00\,(\mathrm{cm\,s}^{-1})$ and $u_f = 4.91\,(\mathrm{cm\,s}^{-1})$ for $\theta = 5^\circ$ and $\theta = 10^\circ$, respectively. The LES simulations predict frontal velocities of $u_f = 4.30\,(\mathrm{cm\,s}^{-1})$ and $u_f = 5.37\,(\mathrm{cm\,s}^{-1})$, showing close agreement with the experimental measurements.

III. Results and Discussion

Fig. 1 illustrates the gravity current produced by a continuous buoyancy flux. In Fig. 1(a), a 2D iso-vorticity map on the center plane highlights the gravity current head (GCH), which is connected to the body of the current through a distinct "neck." At this neck, the velocity u_m reaches its maximum, surpassing the frontal velocity u_f. Fig. 1(b) displays the map of velocity (u), clearly showing the maximum velocity at the neck region. The flowrate profile $q/q_\circ$, shown in Fig. 1(c), reaches its peak at the neck, emphasizing the critical role of this region in feeding the GCH with high-momentum flow.

A. Frontal Speed

Figures 3(b) and 4(b) show the frontal velocity for incline angles of 5° and 10°. The LES results exhibit good agreement with the laboratory observations of Britter and Linden [6]. Both their experimental results and our LES study confirm that the frontal velocity remains independent of the downstream propagation distance, x_f, and is proportional to the buoyancy flux, $g'_\circ q_\circ$. Notably, the frontal velocity remains nearly constant for both slope angles examined in this study, with normalized values of $u_f/(g'_\circ q_\circ)^{(1/3)} = 1.325$ for $\theta = 5^\circ$ and $u_f/(g'_\circ q_\circ)^{(1/3)} = 1.565$ for $\theta = 10^\circ$.

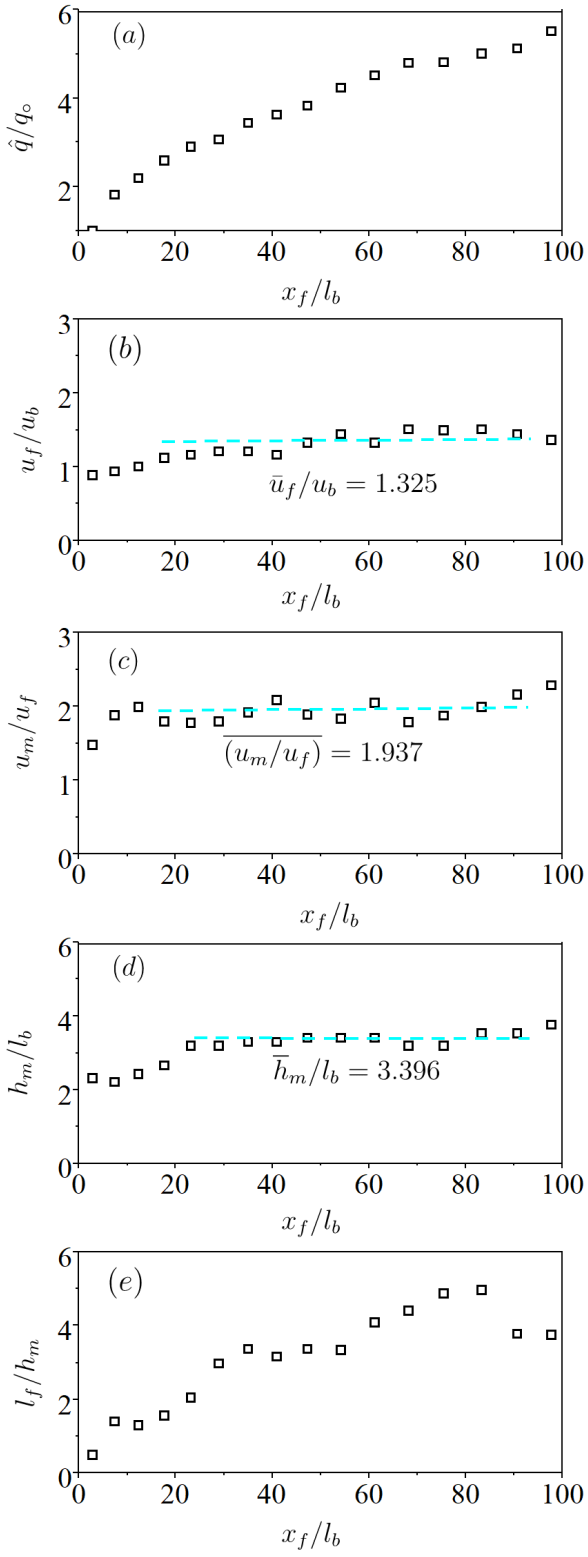

Figure. 3. Key parameters of a gravity current produced by a continuous source of buoyancy flux $g'_\circ q_\circ = 0.000041\ m^3/s^3$ down an incline with an angle $\theta = 5^\circ$c. (a) The peak flow rate $\hat{q}/q_\circ$. (b) the frontal velocity u_f/u_b, in which $u_b = (g'_\circ q_\circ)^{(1/3)}$. (c) The maximum-to-frontal velocity ratio u_m/u_f. (e) The dimensionless GCH height h_m/l_b. (d) The GCH length-to-height ratio l_f/h_m. The length scale is $l_b = [q_\circ^2/g']^{\frac{1}{3}}$.

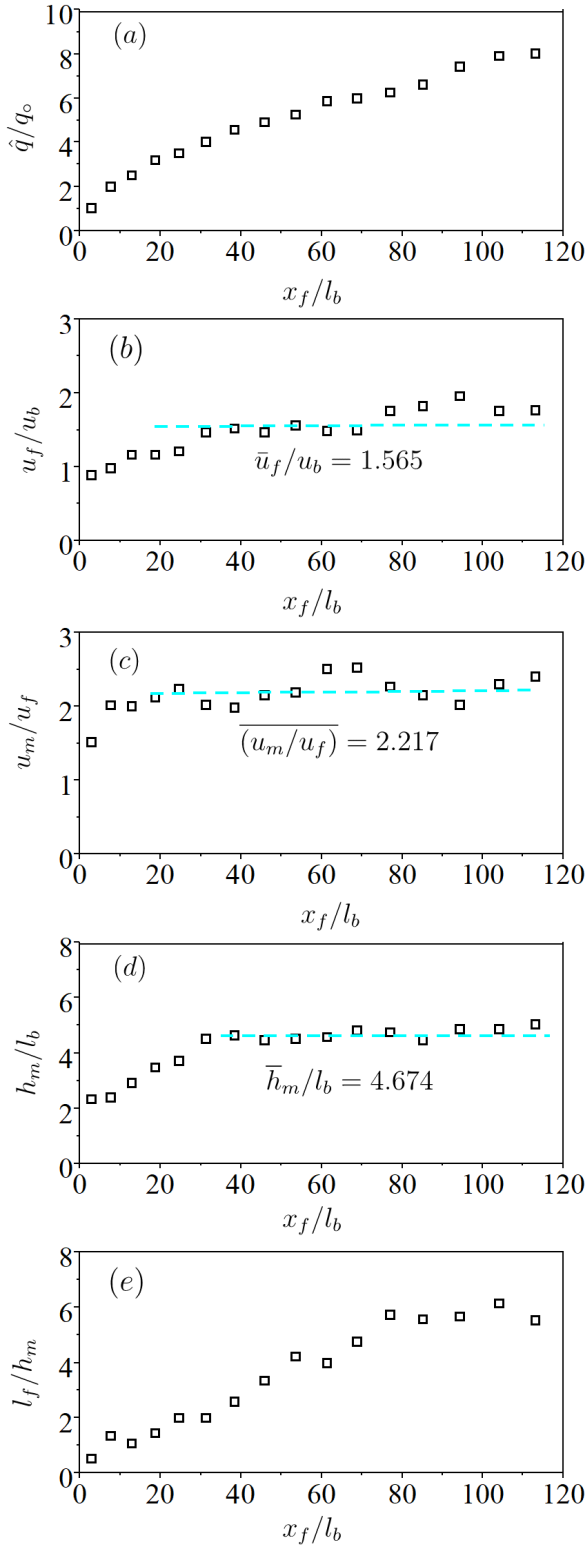

Figure. 4. Key parameters of a gravity current produced by a continuous source of buoyancy flux $g'_\circ q_\circ = 0.000041\ m^3/s^3$ down an incline with an angle $\theta = 10°$c. (a) The peak flow rate $\hat{q}/q_\circ$. (b) the frontal velocity u_f/u_b, in which $u_b = (g'_\circ q_\circ)^{(1/3)}$. (c) The maximum-to-frontal velocity ratio u_m/u_f. (e) The dimensionless GCH height h_m/l_b. (d) The GCH length-to-height ratio l_f/h_m. The length scale is $l_b = [q_o^2/g']^{\frac{1}{3}}$.

B. Peak flow Rate

The continuous source of buoyancy flux produces an unsteady density current with a flow rate

$$q(x,t) = \int_0^H u^+(x,y,t)\,dy \tag{3.1}$$

where $u^+(x,y,t) = u(x,y,t)$ if $u(x,y,t) > 0$ and $u^+ = 0$ if $u(x,y,t) \le 0$. Panel (d) in Fig. 1 shows the dimensionless flow profiles, $q(x,t)/q_\circ$ versus x, obtained at $t/t^* = 8$ for the gravity current propagating over an inclined plane with a slope of 10°. A peak discharge, $\hat{q}(x,t)$, is observed at a neck through which the gravity current head (GCH) connects to the dam-break flow feeding from behind. Figs. 3(a) and 4(a) illustrate the dimensionless peak flow rate $\hat{q}/q_\circ$ at the neck and its dependence on the dimensionless frontal position x_f/l_b. The length scale is $l_b = [q_o^2/g']^{\frac{1}{3}}$. The peak flow rate increases as the current propagates along the slope due to both the entrainment of surrounding fluid into the head and the continuous addition of fluid from the trailing current. This increase is more significant for $\theta = 10°$ compared to $\theta = 5°$, as the steeper slope enhances flow acceleration and mixing.

C. Maximum Velocity

The maximum velocity, u_m, occurs near the same location as the peak flow rate. Figures 3(c) and 4(c) show the ratio of maximum to front velocity, u_m/u_f, for slopes of $\theta = 5°$ and $\theta = 10°$. For $\theta = 5°$, the maximum velocity u_m is 93.7% greater than the frontal velocity, with $u_m/u_f = 1.937$. For $\theta = 10°$, the ratio increases slightly to $u_m/u_f = 2.217$.

D. Dimensions of the Head

The height of the gravity current head (GCH), h_m, is defined as the elevation at the center of the Kelvin–Helmholtz vortex, where the vorticity peaks. The length of the GCH, l_f, is the distance from the front to the back, where the maximum velocity occurs at the neck.

Figures 3(e) and 4(e) show the length-to-height ratio of the head for $\theta = 5°$ and $\theta = 10°$, which increases initially and then approaches a constant as the current advances down the incline. This observation is consistent with the findings of Britter and Linden (1980) [6]. The head expands as it moves down the incline due to both direct entrainment into the head and the continuous inflow of fluid from the trailing current.

However, the height of the current stays remarkably constant over the entire length of the channel on the incline. Figs. 3(d) and 4(d) illustrate the height, reaching a value of $h_m/l_b = 3.396$ for $\theta = 5°$ and a higher value of $h_m/l_b = 4.674$ for $\theta = 10°$, attributable to increased entrainment on the steeper slope.

The LES has provided a wealth of data that remains to be analyzed. We shall further examine the turbulent entrainment process of the gravity current in a follow-up study.

IV. Conclusion

The large-eddy simulations (LES) conducted in this study successfully captured the dynamics of gravity currents generated by a continuous buoyancy flux on an inclined slope. A raised gravity current head (GCH) forms at the leading edge of the current due to the development of Kelvin–Helmholtz instabilities. The most significant flow occurs at the back of the GCH through a neck connecting the head to the body of the trailing current.

While previous studies focused primarily on determining the front velocity, this study emphasizes the flow through the neck, which is crucial in sustaining the GCH and its impact on offshore coastal structures and sediment resuspension on the seafloor. The results show the simulated front velocity aligns well with laboratory observations. Additionally, the LES revealed that the velocity at the neck –not measured in laboratory experiments – exceeds the frontal velocity by factors of 1.94 and 2.22 for slope angles of 5° and 10°, respectively.

As the current propagates down the slope, the peak flow rate increases and the GCH grows in size due to both the entrainment of surrounding fluid and continuous addition of fluid from the trailing current. This growth is more pronounced at a steeper slope ($\theta = 10°$) compared to the shallower slope ($\theta = 5°$), indicating the influence of slope on entrainment and flow dynamics. These findings enhance our understanding of inclined gravity currents and provide a foundation for future studies on their impact on offshore structures and sediment transport.

Acknowledgment

This research is supported by the Natural Sciences and Engineering Research Council of Canada under Grant RGPIN-2019- 05776, a MEDA Scholarship and a FRQNT Scholarship to Sana Ramezani.

References

[1] S.K. Hsu, J. Kuo, L. Chung-Liang, T. Ching-Hui, W.B. Doo, C.Y. Ku, and J.C Sibuet, "Turbidity currents, submarine landslides and the 2006 Pingtung earthquake off SW Taiwan," TAO: Terrestrial, Atmospheric and Oceanic Sciences, vol. 19, no. 6, pp. 767-772, 2008.

[2] Bruce CharlesHeezen and William Maurice Ewing "Turbidity currents and submarine slumps, and the 1929 grand banks [newfoundland] earthquake," American journal of Science, vol. 250, no. 12, pp. 849-873, 1952.

[3] Peiwei Xie, Yan Du and Vincent H. Chu, "Impact forces by a gravity current on a circular cylinder above the seabed," Applied Ocean Research, vol. 125, no. 103243, pp. 1-, 2022.

[4] Sana Ramezani, Peiwei Xie and Vincent H. Chu, "Impact force of non-boussinesq gravity-current head against a circular cylinder above the seabed," Applied Ocean Research, vol. 145, no. 103939, pp. 1-18, 2024.

[5] Ryan J. Lowe, James W. Rottman and Paul F. Linden, "The non-Boussinesq lock-exchange problem. Part 1. Theory and experiments," Journal of Fluid Mechanics, vol. 537, pp. 101–124, 2005.

[6] R. E. Britter and P. F. Linden, "The motion of the front of a gravity current travelling down an incline," J. of Fluid Mechanics, vol. 99, pp. 531-543, 1980.

[7] H. G. Weller, G. Tabor, H. Jasak, and C. Fureby, "A tensorial approach to computational continuum mechanics using object-oriented techniques," *Computers in Physics*, vol. 12, no. 6, pp. 620–631, 1998.

[8] C. J. Greenshields, "OpenFOAM User Guide, Version 7," OpenFOAM Foundation Ltd, 2019.

[9] P. Higuera, J. L. Lara, and I. J. Losada, "Simulating coastal engineering processes with OpenFOAM®," *Coastal Engineering*, vol. 71, pp. 119–134, 2013.

[10] P. Higuera, J. L. Lara, and I. J. Losada, "Three-dimensional interaction of waves and porous coastal structures using OpenFOAM®. Part I: Formulation and validation," *Coastal Engineering*, vol. 83, pp. 243–258, 2014.

[11] P. Higuera, J. L. Lara, and I. J. Losada, "Three-dimensional interaction of waves and porous coastal structures using OpenFOAM®. Part II: Application," *Coastal Engineering*, vol. 83, pp. 259–270, 2014.

[12] V. T. Nguyen, "3D numerical simulation of free surface flows over hydraulic structures in natural channels and rivers," *Applied Mathematical Modelling*, vol. 39, no. 20, pp. 6285–6306, 2015.

[13] R. Nicole, "Title of paper with only first word capitalized," J. Name Stand. Abbrev., in press.

[14] Y. Yorozu, M. Hirano, K. Oka, and Y. Tagawa, "Electron spectroscopy studies on magneto-optical media and plastic substrate interface," IEEE Transl. J. Magn. Japan, vol. 2, pp. 740–741, August 1987 [Digests 9th Annual Conf. Magnetics Japan, p. 301, 1982].

[15] M. Young, The Technical Writer's Handbook. Mill Valley, CA: University Science, 1989.

[16] M. F. Gruber, C. J. Johnson, C. Y. Tang, M. H. Jensen, L. Yde, and C. Hélix-Nielsen, "Computational fluid dynamics simulations of flow and concentration polarization in forward osmosis membrane systems," *J. Membr. Sci.*, vol. 379, no. 1–2, pp. 488–495, 2011.

[17] R. Krpan and B. Končar, "Simulation of turbulent wake at mixing of two confined horizontal flows," *Sci. Technol. Nucl. Install.*, vol. 2018, 2018.

[18] A. Yoshizawa, "A statistically-derived subgrid model for the large-eddy simulation of turbulence," *Phys. Fluids*, vol. 25, no. 9, pp. 1532–1538, 1982.

[19] A. Yoshizawa and K. Horiuti, "A statistically-derived subgrid-scale kinetic energy model for the large-eddy simulation of turbulent flows," *J. Phys. Soc. Jpn.*, vol. 54, no. 8, 1985.

[20] E. V. Ermanyuk and N. V. Gavrilov, "Interaction of an internal gravity current with a submerged circular cylinder," *J. Appl. Mech. Tech. Phys.*, vol. 46, no. 2, pp. 216–223,

[21] J. O. Shin, S. B. Dalziel, and P. F. Linden, "Gravity currents produced by lock exchange," *J. Fluid Mech.*, vol. 521, pp. 1–34, 2004.

[22] W. Rodi, G. Constantinescu, and T. Stoesser, *Large-Eddy Simulation in Hydraulics*. Boca Raton, FL: CRC Press, 2013.

[23] L. Davidson, *Fluid Mechanics, Turbulent Flow, and Turbulence Modeling*. Gothenburg, Sweden: Chalmers University of Technology, 2015.